

A Scalable Microstructure Photonic Coating Fabricated by Roll-to-Roll “Defects” for Daytime Subambient Passive Radiative Cooling

Sipan Liu,[@] Chenxi Sui,[@] Myers Harbinson, Michael Pudlo, Himendra Perera, Zhenzhen Zhang, Ruguan Liu, Zahyun Ku, Md Didarul Islam, Yuxuan Liu, Ronghui Wu, Yong Zhu, Jan Genzer, Saad A. Khan, Po-Chun Hsu,^{*} and Jong Eun Ryu^{*}



Cite This: <https://doi.org/10.1021/acs.nanolett.3c00111>



Read Online

ACCESS |



Metrics & More



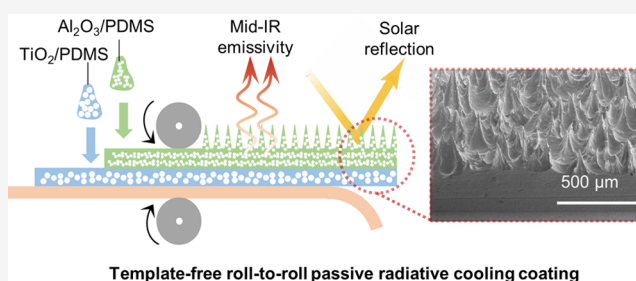
Article Recommendations



Supporting Information

ABSTRACT: The deep space’s coldness (~ 4 K) provides a ubiquitous and inexhaustible thermodynamic resource to suppress the cooling energy consumption. However, it is nontrivial to achieve subambient radiative cooling during daytime under strong direct sunlight, which requires rational and delicate photonic design for simultaneous high solar reflectivity ($>94\%$) and thermal emissivity. A great challenge arises when trying to meet such strict photonic microstructure requirements while maintaining manufacturing scalability. Herein, we demonstrate a rapid, low-cost, template-free roll-to-roll method to fabricate spike microstructured photonic nanocomposite coatings with Al_2O_3 and TiO_2 nanoparticles embedded that possess 96.0% of solar reflectivity and 97.0% of thermal emissivity. When facing direct sunlight in the spring of Chicago (average 699 W/m^2 solar intensity), the coatings show a radiative cooling power of 39.1 W/m^2 . Combined with the coatings’ superhydrophobic and contamination resistance merits, the potential 14.4% cooling energy-saving capability is numerically demonstrated across the United States.

KEYWORDS: nanocomposite, subambient daytime cooling, passive radiative cooling, scalable photonic structure



Climate change has severely impacted people’s lives and the environment. Because of the rising temperature, approximately 20.3% of electrical energy was used in the building cooling system for the US residence and commercial buildings,^{1,2} presenting a challenge toward a sustainable future. Passive radiative cooling (PRC) materials can mitigate cooling consumption by delivering wireless access to the cold thermodynamic resources (~ 4 K) in deep space.^{3–11} By reflecting solar radiation and radiating heat into the cold universe through the atmospheric transparent window, the radiative cooling materials can achieve noticeable cooling energy savings under direct sunlight. The ideal radiative cooling materials should simultaneously possess high cooling power, low cost, scalable manufacturing, and contamination resistance characteristics. Previous research showed that rough microstructures could achieve high cooling power and anticontamination because the rough surfaces elevate the thermal emissivity by creating a gradual refractive index change and generating a superhydrophobic surface.^{3,12–15} However, nontriviality arises when fabricating the desired microstructures with low cost and scalability because high mid-infrared (mid-IR) emissivity requires high-precision control of the photonic microstructures, where costly and low-yield microfabrication techniques are generally employed (such as photolithography and imprinting).^{3,12–15} Thus, innovative manufacturing methods need to be developed to fabricate

these microstructures for large-scale applications, such as building energy savings.

Roll-to-roll has been an industrial-level process for scalable and inexpensive thin-film fabrication. Zhai et al. first used the roll-to-roll method to fabricate flat SiO_2 /polymethylpentene nanocomposite film with a silver reflection layer to obtain a solar reflectance of 96% and a mid-infrared emissivity of 93%. However, the e-beam metal evaporation silver layer significantly increases the manufacturing cost and time.⁵ Zhou et al. directly coated a flat polydimethylsiloxane (PDMS) layer on the metal sheet by the roll-to-roll method, which can avoid the expensive metal evaporation process. However, the performance and cost were limited by the metal substrate.¹⁶ The common ribbon and spike defects in traditional roll-to-roll manufacturing inspired researchers to develop a novel scalable way to fabricate periodical microstructures.^{17–20} Specifically, the positive pressure gradient generated in the downstream meniscus sows the seeds of the spike “defects” on the

Received: January 9, 2023

Revised: June 30, 2023

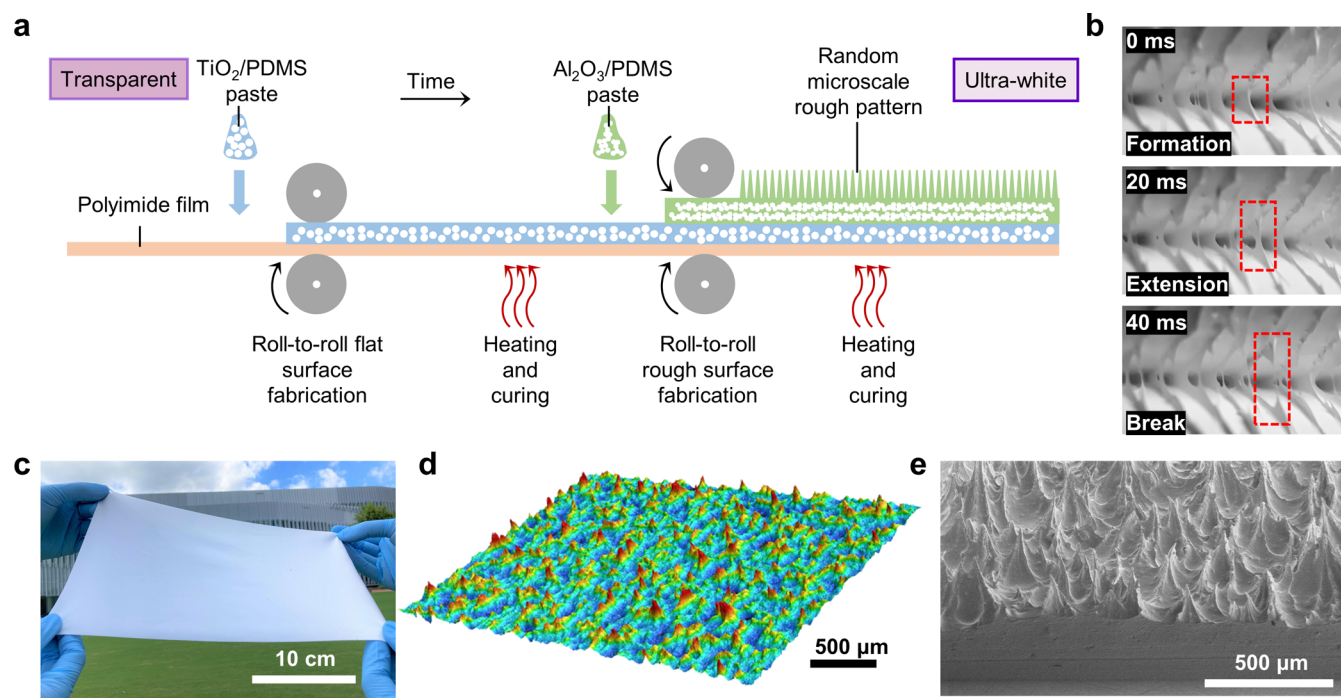


Figure 1. (a) Schematic of the bilayer nanocomposite microstructure photonic coating fabrication. (b) Spike formation schematic during the roll-to-roll fabrication process (15 vol % Al₂O₃/PDMS with relatively low viscosity and low roller speed are utilized for convenient photography, which is not the final product). (c–e) Bilayer products (26 vol % Al₂O₃/PDMS–25 vol % TiO₂/PDMS) sample. (c) Photonic coating photograph. (d) Laser confocal picture of the photonic coating surface. (e) SEM picture of the photonic coating with a cross-section view.

surface.^{21–23} These defects can be robustly kept when the material's rheological properties are modified by adding nanoparticles. In this situation, the defects' peak pitch length is correlated to material properties (i.e., surface energy and viscosity) and fabrication parameters (i.e., roller radius, roller gap, and roller speed).^{24–26} The optimized spike microstructures for high cooling performance can be obtained by manipulating the embedded nanoparticles and fabrication parameters. In addition, metal oxide nanoparticles can reflect sunlight due to the particles' intense backscattering,^{27–29} which potentially enhances the daytime radiative cooling power. Therefore, the modified roll-to-roll manufacturing method could be a cost-effective candidate for fabricating high-performance daytime radiative cooling photonic structures on a large scale.

In this study, we first demonstrated a template-free roll-to-roll method combined with polymeric nanocomposites to fabricate photonic spike coatings for daytime radiative cooling (Figure 1a–e, Figures S1 and S2, Supporting Information Section 2 (SI 2)). A bilayer structure comprising Al₂O₃/polydimethylsiloxane (PDMS) and TiO₂/PDMS enhances the reflectivity of ultraviolet (UV) light (Figure 2a).³⁰ The fabricated photonic coatings show a directional emittance in the mid-IR region of 97.0% and a state-of-the-art substrate-independent solar radiation directional reflectance of 96.0% (Figure 2b). The photonic coating generates a subambient cooling power as high as 39.1 W/m² in the daytime of Chicago with a 0.125 cloud cover ratio. The building energy modeling result shows a 14.4% cooling system energy (31.7 GJ/year) saving capability across the U.S. Compared with the state-of-the-art radiative cooling materials (Figure 2c, SI 3 and 4, normalized in the same weather condition based on May 4 in Chicago, IL), our photonics coating possesses a high solar reflectivity, thermal emissivity, and cooling power.^{3–8,31}

Besides, the photonic coating possesses superhydrophobic merit (water contact angle = 156°), promoting contamination resistance (Figure 2d and Figure S3).

The ideal radiative cooling materials should possess high solar reflectivity and thermal emissivity. The transparent PDMS is used for high thermal emission. TiO₂ and Al₂O₃ nanoparticles are mixed with PDMS to enhance solar reflectivity. TiO₂ is a commercial white painting material with high reflectivity at a thin thickness due to its high refractive index (~2.7). However, the TiO₂ highly absorbs the UV and blue light due to the 3.0 eV bandgap (413 nm), which limits the solar reflectivity around 91%.³² Therefore, low-cost Al₂O₃ nanoparticles are introduced to suppress UV absorptivity to tackle this challenge.³⁰ The final design of the bilayer photonic materials is shown in Figures 1a and 2a. The Al₂O₃/PDMS is layered on top of the TiO₂/PDMS to prevent the UV absorption of TiO₂. Theoretically, larger backscattering coefficients of the nanoparticles lead to higher reflectivity. To validate this, the backscattering coefficients of the nanoparticles were calculated by Mie's theory (Figures 3a,b and Figure S4, SI 6). The selection of 500 nm sized TiO₂ particles was based on their strong backscattering coefficient peak aligning with the peak of solar radiation at 500 nm. For the 200 nm sized Al₂O₃ particles, they were chosen due to their high backscattering coefficient in the UV range and improved processability in PDMS compared to particles of size 100 nm.

Apart from the improved solar reflectivity, we elevated the thermal emissivity by fabricating the spike microstructures on the top surface of the coating. The spike microstructures (~30 μm lateral length) only had a negligible effect on the solar spectrum reflectivity according to the rigorous coupled-wave analysis (RCWA) simulation (Figure 3c) because of the large mismatch between the wavelength of the incident light and the structure size (Figure 3c, SI 8). The spike microstructures

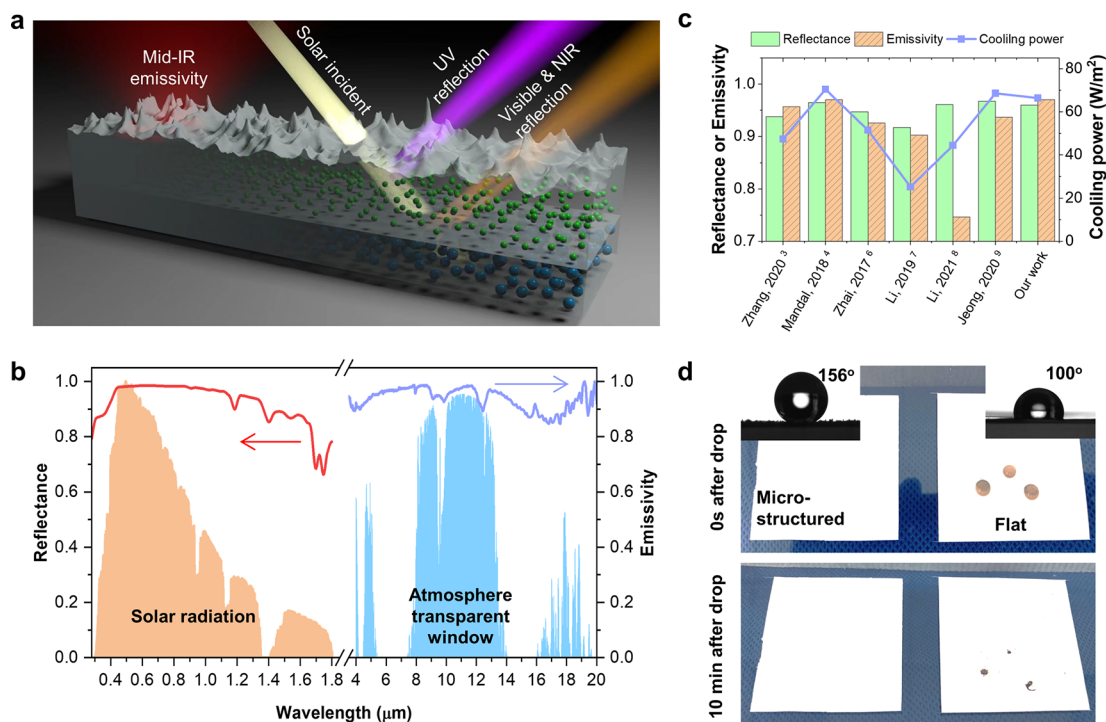


Figure 2. (a) Schematic of the bilayer photonic coating passive radiative cooling, including mid-IR emittance and separately governing the UV light. The smaller green spheres are Al_2O_3 , and larger blue spheres are TiO_2 . (b) Spectral reflectance and emissivity of the photonics coating (bilayer, thickness is $300\ \mu\text{m}$) presenting against normalized ASTM G173-03 reference global tilt solar spectra and a mid-IR transparent window in Chicago, IL. (c) Comparing the solar reflectance, emissivity, and theoretical cooling power (normalized in the same ASTM G173-03 reference global tilt solar spectra and weather conditions in Chicago, IL, by MODTRAN) with the state-of-the-art radiative cooling materials record in refs 3–9. (d) Photonic coating's superhydrophobicity (water contact angle = 156°) and contamination resistance demonstration with a 30° slope (side-view picture in Figure S3).

create a gradual refractive index change at the air/coating interface, which enhances the thermal emissivity.³ The enhancement of the thermal emissivity by the photonic microstructures was simulated by finite element analysis (FEA, COMSOL Multiphysics 5.5, SI 9). The FEA demonstrates that the microstructures significantly increase the hemisphere emissivity from 70.8% (flat PDMS, f-P) to 87.0% (triangular microstructured PDMS, t-P) in the mid-IR region (Figure 3d, SI 9). The triangular microstructure also shows higher emissivity than square and circular topographies (Figures S9 and S10). Boosted by the strong mid-IR absorption of Al_2O_3 or TiO_2 nanoparticles (25 vol % particle concentration), the emissivity can be promoted further to 92.9% (Figures 3d and S11). The simulation results also reveal that the higher height and lower peak pitch length (denser) of the spike lead to a higher emissivity (Figure S12), which guides our roll-to-roll fabrication.

For cooling energy-saving applications, the radiative cooling photonic coating materials must be fabricated on a large scale. The rapid roll-to-roll method fabricates the TiO_2 /PDMS and Al_2O_3 /PDMS bilayer photonic coating materials with spike microstructures by employing viscoelastic fluid instability. The formation of the spike peaks is described in Figure 1b and Video S1 (15 vol % Al_2O_3 /PDMS, relatively low viscosity material, and low roller speed were utilized for convenient photography; it is not final products). Our previous simulation research demonstrated that surface energy γ , viscosity η (or complex viscosity η^*), roller radius R , roller gap d , and roller speed U were strongly correlated to the pressure gradient in the flow direction, which directly led to the formation of the

spike “defects”.²³ To demonstrate the effects of η , U , γ , and R/d on the final spikes' peak pitch length (p_{spike}), parametric experiments are conducted with U ranging from 20 to 100 rpm and R/d from 100 to 320. The 4–24 vol % Al_2O_3 /PDMS nanocomposites are prepared for different viscosities. The γ and η^* measurement results of the nanocomposites are shown in Figure 3e,f, SI 10. The parametric roll-to-roll experiment results demonstrate that the higher η (higher particle content), U , and R/d would lead to a smaller p_{spike} as shown in Figure 3g and Table S5. The Capillary number ($Ca = \eta U/\gamma$, used to be the index for predicting the critical point of the roll-to-roll defect appearance, but the fabrication in this study is far beyond the critical point) could not fit the viscoelastic fluid fabrication very well (Figure S15). We propose a novel roll-to-roll defects coefficient, $\text{RDC} = ((\eta/\gamma)^{1/3}UR/d)^{-0.5}$, to fit with the p_{spike} . The p_{spike} vs RDC result is shown in Figure 3h. A linear proportion shows that the p_{spike} decreased as the RDC decreased.

In the final bilayer products, a flat 25 vol % TiO_2 /PDMS is first roll-to-roll fabricated and cured. Then, the top layer is fabricated on the flat layer by the roll-to-roll method, where 26 vol % Al_2O_3 and 3 vol % SiO_2 (10 nm, stabilization particles) are mixed into PDMS to achieve close-boundary viscosity but with processability. When the U went to 100 rpm and the R/d went to 320, $\sim 100\ \mu\text{m}$ p_{spike} is achieved (Figure 1d,e), which is desired for improving thermal emissivity (Figure 1d,e).

It is necessary to characterize the optical properties of solar and mid-IR ranges to prove the radiative cooling capability of the photonic coating. The ultraviolet–visible (UV–vis) and Fourier transform infrared (FTIR) spectrometers characterize

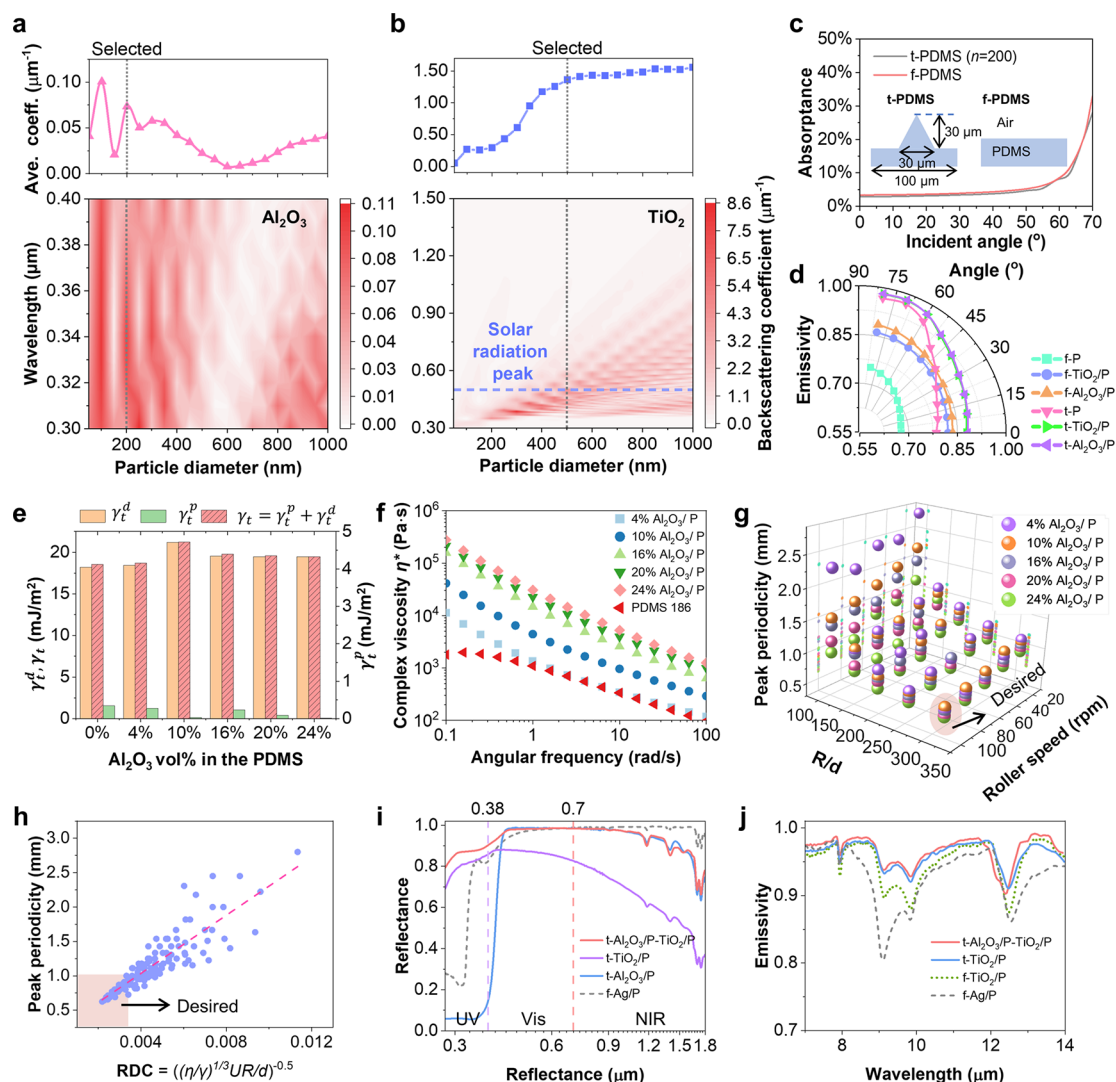


Figure 3. (a, b) Nanoparticle/PDMS backscattering coefficients calculation by Mie's theory (particle concentrations were 25 vol %, "Selected" marked the particles size in the final product). (a) Al_2O_3 nanoparticles' average backscattering coefficient and the backscattering coefficient along the change of the particle diameter and wavelength in the UV range. (b) TiO_2 nanoparticles' average backscattering coefficient and the backscattering coefficient along the change of the particle diameter and wavelength in the solar spectral range. (c) Spike microstructure's effect on solar spectral reflectance and the models in the RWAC model. In the legend, "t" is a triangular spike model and "f" is the flat model. (d) Enhancement results for the mid-IR emissivity by the photonic microstructures simulated by finite elements analysis (FEA, COMSOL); the particle concentration was 25 vol %. In the legend, P is PDMS. (e) Surface energy components (polar, γ_t^d , disperse, γ_t^p , total, $\gamma_t = \gamma_t^d + \gamma_t^p$) of the different Al_2O_3 (200 nm) particle concentrations in PDMS (P). (f) Complex viscosity (η^*) vs angular frequency. (g) A parametric experiment of the nanocomposite pastes. Peak pitch length (p_{peak}) vs roller geometry factor (R/d) and roller speed (U). (h) Peak pitch length vs roll-to-roll defects coefficient (RDC). (i) Reflectance of a photonic coating sample (t- Al_2O_3 /P- TiO_2 /P) and other comparing samples on the solar spectrum. (j) Emissivity of the photonic coating and other comparing samples in the mid-IR (7–14 μm) range. In the legend, "t" is spike microstructured coating, "f" is the flat coating, and "P" is PDMS.

solar reflectivity and mid-IR thermal emissivity, respectively. In Figure 3i, the UV–vis results show that the bilayer Al_2O_3 /PDMS- TiO_2 /PDMS coating overcomes the drawbacks of the Al_2O_3 /PDMS (low overall reflectivity, 59.7% with 100 μm thickness) and TiO_2 /PDMS (high absorption at UV, 91.7% solar reflectance with 100 μm thickness). A 96.0% solar reflectivity is achieved, which is comparable with PDMS/silver.³³ The FTIR measurement verified that the spike structure enhanced the mid-IR emission (Figure 3j). The 97.0% and 96.5% emissivity are obtained from the structured bilayer Al_2O_3 /PDMS- TiO_2 /PDMS and the structured TiO_2 /PDMS samples, respectively. The referenced materials, flat

TiO_2 /PDMS and flat PDMS, achieve 95.0% and 93.2% emissivity, respectively.

To assess the daytime radiative cooling performance of the sample, a Peltier-based radiative cooling power measurement platform was established near Lake Michigan in Chicago, IL (Figure S16). The temperature drop measurement setup was positioned on a rooftop at Chicago University, Chicago, IL (Figure S17). The outdoor measurements took place in Chicago on May 4, 2023. The measurement system depicted in Figure 4a–c consisted of a Peltier device, a PID controller, a data acquisition (DAQ) system, a power supply, a thermopile pyranometer, and a device for measuring the sample temperature. The theoretical calculations were conducted

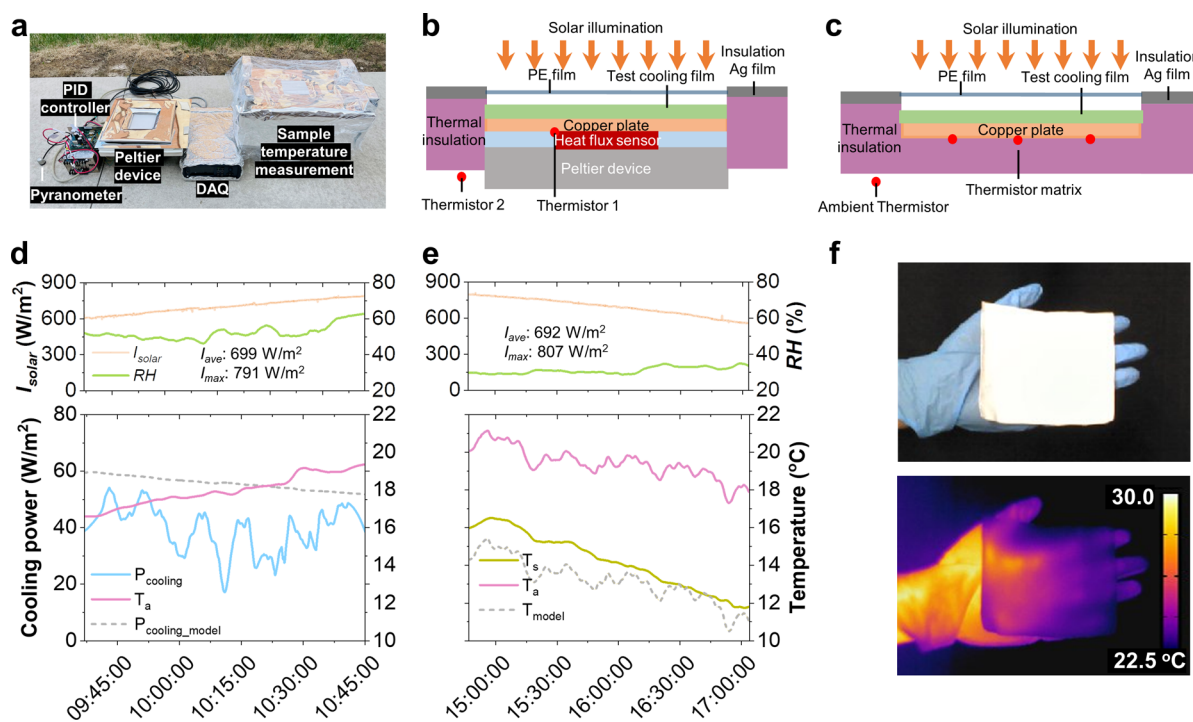


Figure 4. (a) Outdoor cooling power and temperature-drop measurement platforms. (b) Schematic of the Peltier-based measurement platform. (c) Schematic of the temperature-drop measurement platform. (d) Bilayer photonic coatings cooling power (P_{cooling}) measurement result and theoretical model prediction cooling power ($P_{\text{cooling_model}}$) with corresponding relative humidity (RH), ambient temperature (T_a), and solar illumination (I_{solar} average and maximum illumination are I_{ave} and I_{max} , respectively). (e) Bilayer photonic coatings temperature measurement result (T_s) and model predicted temperature (T_{model}) with corresponding RH, T_a , and I_{solar} . (f) Infrared thermal camera pictures of bilayer photonic coating on the author's hand.

based on the model proposed by Aili.³⁴ For these calculations, temperature and humidity data were obtained from field test measurements, the heat transfer coefficient was estimated as 10 W/(m² K), and the cloud cover rate 0.125 was cited from National Oceanic and Atmospheric Administration's (NOAA) National Weather Service (NWS)—Chicago O'Hare International Airport weather record.³⁵ The Al₂O₃/PDMS-TiO₂/PDMS coating demonstrated an average cooling power of 39.1 W/m² from 9:37 AM to 10:45 AM, as determined from the field test. This value was slightly lower than the theoretical calculation result of 55.1 W/m², as shown in Figures 4d and S18. The deviation between the field test and theoretical calculation may be attributed to factors such as the estimated cloud cover rate and parasitic heat loss (heat convection and conduction) from the test platform. With regard to the temperature-drop test, the same sample exhibited an average temperature drop of 5.2 °C, slightly lower than the theoretical model calculation of 6.2 °C, as depicted in Figures 4e and S18.

The infrared camera image clearly illustrates the excellent thermal emissivity of the coating, allowing for effective dissipation of the heat beneath the sample (Figure 4f). To demonstrate the outdoor UV durability of the coating, one-year equivalent solar light UV radiation was applied to the coating continually. The results demonstrated no significant mechanical strength or optical properties degradation after one-year equivalent solar light UV radiation (Figures S19 and S20).

Inspired by the radiative cooling, UV resistance, and self-cleaning capability, we proposed that the bilayer photonic coatings can serve as the efficient radiative coatings of the roofs for cooling energy savings in buildings (Figure 5a). To

quantitatively assess the scale-up impact of photonic coatings on building cooling efficiency, we utilized EnergyPlus, incorporating experimentally measured optical properties of the materials. This allowed us to simulate the potential energy savings in cooling throughout the year for midrise apartments across various locations in the United States. Fifteen cities corresponding to 15 climate zones in the U.S. were chosen to calculate the cooling energy consumption.^{6,33,36} Compared with the baseline, buildings with radiative cooling roofs save energy up to 65.25 GJ/year in Phoenix, which constitutes 11.1% of the year-round cooling energy in the baseline buildings (Figure 5b). As shown in the cooling energy saving map (Figure 5c), the cooling materials benefit more in the hot and dry areas: 54.66 GJ/year in Honolulu (climate zone number: 1A), 45.1 GJ/year in Austin (2A), 65.24 GJ/year in Phoenix (2B), and 40.8 GJ/year in Los Angeles (3B). Even if the temperature and solar radiation are high in these areas, the radiative cooling materials perform better because they reflect sunlight nearly perfectly and radiate more heat to the deep universe. However, the saving amount gradually decreases when the cooling materials are exposed to the weather in the cold areas: 9.3 GJ/year in Fairbanks (8) and 14.5 GJ/year in Duluth (7). It is because the cooling load is small in cold weather. Because the radiative photonic coating provides all-day cooling power when space cooling is needed,³³ by applying our radiative cooling photonic coatings to rooftops, an estimated average annual energy savings of approximately 31.7 GJ/year could be achieved across the entire United States. This accounts for approximately 14.4% of the total cooling energy consumed throughout the year in the United States.

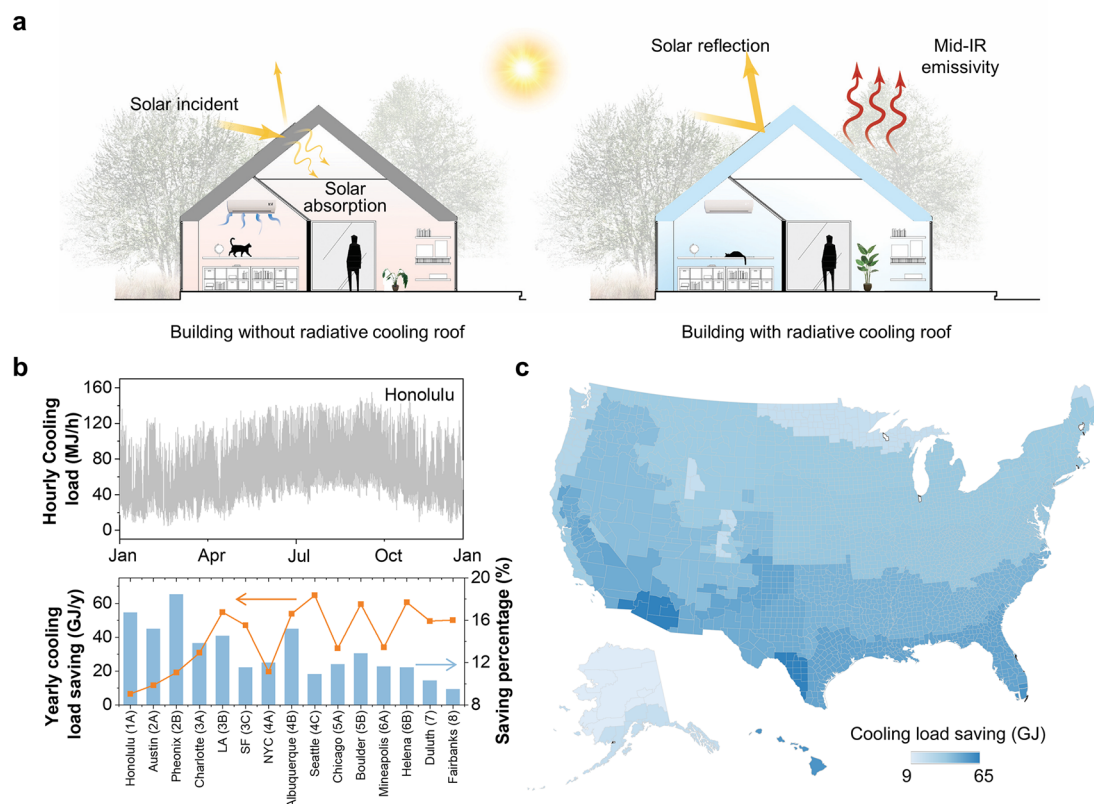


Figure 5. (a) Schematic of the photonic coating applied on building cooling. (b) Building cooling energy saving simulation results in 15 cities corresponding to 15 climate zones in the US compared with the baseline buildings (Honolulu as 1A climate zone example). (c) Cooling energy savings map of the United States.

In this study, we employed a cost-effective and scalable approach, the roll-to-roll method, to fabricate high-performance passive radiative cooling microstructured photonic coatings. Through careful control of the nanocomposite's viscosity and fabrication parameters such as roller gap and speeds, we successfully generated periodic spike microstructures during the roll-to-roll process. These microstructures endowed the materials with remarkable properties, including 97.0% emissivity and strong self-cleaning capability.

To predict the peak pitch length based on the viscoelastic properties of the materials and fabrication parameters, we proposed a novel metric called roll-to-roll defect coefficient (RDC). The photonic coating exhibited an average cooling power of 39.1 W/m^2 under direct sunlight. Leveraging its high cooling power, scalability in fabrication, and superhydrophobic characteristics, the coating was proposed as an effective solution for cooling roofs. Numerical simulations demonstrated a significant potential for year-round energy savings, with approximately 14.4% of building cooling energy consumption in the United States being mitigated.

Furthermore, this fabrication method is adaptable to a wide range of viscous composite pastes, enabling the scalable application of photonic coatings. The findings of this research not only offer a promising platform for expanding the application of traditional roll-to-roll fabrication but also serve as inspiration for technological advancements in radiative cooling materials.

■ ASSOCIATED CONTENT

SI Supporting Information

The Supporting Information is available free of charge at <https://pubs.acs.org/doi/10.1021/acs.nanolett.3c00111>.

Additional experimental details, materials, and methods, including photographs of experimental setup (PDF)

Video S1: spike formation slow-motion movie (MOV)

■ AUTHOR INFORMATION

Corresponding Authors

Po-Chun Hsu – Pritzker School of Molecular Engineering, University of Chicago, Chicago, Illinois 60637, United States; Department of Mechanical Engineering and Materials Science, Duke University, Durham, North Carolina 27603, United States; orcid.org/0000-0002-6509-9377; Email: pochunhsu@uchicago.edu

Jong Eun Ryu – Department of Mechanical and Aerospace Engineering, North Carolina State University, Raleigh, North Carolina 27603, United States; orcid.org/0000-0002-8238-9130; Email: jryu@ncsu.edu

Authors

Sipan Liu – Department of Mechanical and Aerospace Engineering, North Carolina State University, Raleigh, North Carolina 27603, United States; orcid.org/0000-0003-3446-5896

Chenxi Sui – Pritzker School of Molecular Engineering, University of Chicago, Chicago, Illinois 60637, United States; Department of Mechanical Engineering and Materials

Science, Duke University, Durham, North Carolina 27603, United States

Myers Harbinson – Department of Mechanical and Aerospace Engineering, North Carolina State University, Raleigh, North Carolina 27603, United States

Michael Pudlo – Department of Mechanical and Aerospace Engineering, North Carolina State University, Raleigh, North Carolina 27603, United States

Himendra Perera – Department of Chemical and Biomolecular Engineering, North Carolina State University, Raleigh, North Carolina 27603, United States; orcid.org/0000-0003-2749-2028

Zhenzhen Zhang – Revibe Technologies, Wake Forest, North Carolina 27587, United States

Ruguan Liu – Robotics Department, Amazon, Inc., Westborough, Massachusetts 01581, United States

Zahyun Ku – Materials and Manufacturing Directorate, Air Force Research Laboratory, WPAFB, Ohio 45433, United States

Md Didarul Islam – Department of Mechanical and Aerospace Engineering, North Carolina State University, Raleigh, North Carolina 27603, United States

Yuxuan Liu – Department of Mechanical and Aerospace Engineering, North Carolina State University, Raleigh, North Carolina 27603, United States; orcid.org/0000-0001-8196-1054

Ronghui Wu – Pritzker School of Molecular Engineering, University of Chicago, Chicago, Illinois 60637, United States; Department of Mechanical Engineering and Materials Science, Duke University, Durham, North Carolina 27603, United States

Yong Zhu – Department of Mechanical and Aerospace Engineering, North Carolina State University, Raleigh, North Carolina 27603, United States

Jan Genzer – Department of Chemical and Biomolecular Engineering, North Carolina State University, Raleigh, North Carolina 27603, United States

Saad A. Khan – Department of Chemical and Biomolecular Engineering, North Carolina State University, Raleigh, North Carolina 27603, United States; orcid.org/0000-0002-1530-8249

Complete contact information is available at: <https://pubs.acs.org/10.1021/acs.nanolett.3c00111>

Author Contributions

@S.L. and C.S. contributed equally to this work.

Notes

The authors declare no competing financial interest.

ACKNOWLEDGMENTS

This research is based upon work supported by the start-up fund by Pratt School of Engineering, Duke University (P.H.), NCSU Faculty Research and Professional Development award (J.R.), and National Science Foundation under Grant No. 2031558. Part of this work was performed at the Analytical Instrumentation Facility (AIF) at North Carolina State University, supported by the State of North Carolina and the National Science Foundation (Award ECCS-2025064).

ABBREVIATIONS

PRC, passive radiative cooling; mid-IR, mid-infrared; PDMS, polydimethylsiloxane; RCWA, rigorous coupled-wave analysis;

FEA, finite element analysis; RDC, roll-to-roll defects coefficient; UV–vis, ultraviolet–visible; FTIR, Fourier transform infrared.

REFERENCES

- (1) US Department of Energy. 2010 Residential Energy End-Use Expenditure Splits, by Fuel Type. Build. Energy Data B, 2012.
- (2) Chu, S.; Majumdar, A. Opportunities and Challenges for a Sustainable Energy Future. *Nature* **2012**, *488* (7411), 294–303.
- (3) Zhang, H.; Ly, K. C. S.; Liu, X.; Chen, Z.; Yan, M.; Wu, Z.; Wang, X.; Zheng, Y.; Zhou, H.; Fan, T. Biologically Inspired Flexible Photonic Films for Efficient Passive Radiative Cooling. *Proc. Natl. Acad. Sci. U. S. A* **2020**, *117* (26), 14657–14666.
- (4) Mandal, J.; Fu, Y.; Overvig, A. C.; Jia, M.; Sun, K.; Shi, N. N.; Zhou, H.; Xiao, X.; Yu, N.; Yang, Y. Hierarchically Porous Polymer Coatings for Highly Efficient Passive Daytime Radiative Cooling. *Science* **2018**, *362* (6412), 315–319.
- (5) Zhai, Y.; Ma, Y.; David, S. N.; Zhao, D.; Lou, R.; Tan, G.; Yang, R.; Yin, X. Scalable-Manufactured Randomized Glass-Polymer Hybrid Metamaterial for Daytime Radiative Cooling. *Science* **2017**, *355* (6329), 1062–1066.
- (6) Li, T.; Zhai, Y.; He, S.; Gan, W.; Wei, Z.; Heidarinejad, M.; Dalgo, D.; Mi, R.; Zhao, X.; Song, J.; Dai, J.; Chen, C.; Aili, A.; Vellore, A.; Martini, A.; Yang, R.; Srebric, J.; Yin, X.; Hu, L. A Radiative Cooling Structural Material. *Science* **2019**, *364* (6442), 760–763.
- (7) Li, D.; Liu, X.; Li, W.; Lin, Z.; Zhu, B.; Li, Z.; Li, J.; Li, B.; Fan, S.; Xie, J.; Zhu, J. Scalable and Hierarchically Designed Polymer Film as a Selective Thermal Emitter for High-Performance All-Day Radiative Cooling. *Nat. Nanotechnol.* **2021**, *16* (2), 153–158.
- (8) Jeong, S. Y.; Tso, C. Y.; Wong, Y. M.; Chao, C. Y. H.; Huang, B. Daytime Passive Radiative Cooling by Ultra Emissive Bio-Inspired Polymeric Surface. *Sol. Energy Mater. Sol. Cells* **2020**, *206*, No. 110296.
- (9) Raman, A. P.; Anoma, M. A.; Zhu, L.; Rephaeli, E.; Fan, S. Passive Radiative Cooling below Ambient Air Temperature under Direct Sunlight. *Nature* **2014**, *515* (7528), 540–544.
- (10) Hsu, P.-C.; Song, A. Y.; Cattrysse, P. B.; Liu, C.; Peng, Y.; Xie, J.; Fan, S.; Cui, Y. Radiative Human Body Cooling by Nanoporous Polyethylene Textile. *Science* **2016**, *353* (6303), 1019–1023.
- (11) Leroy, A.; Bhatia, B.; Kelsall, C. C.; Castillejo-Cuberos, A.; Di Capua, M. H.; Zhao, L.; Zhang, L.; Guzman, A. M.; Wang, E. N. High-Performance Subambient Radiative Cooling Enabled by Optically Selective and Thermally Insulating Polyethylene Aerogel. *Sci. Adv.* **2019**, *5* (10), No. eaat9480.
- (12) Shi, N. N.; Tsai, C. C.; Camino, F.; Bernard, G. D.; Yu, N.; Wehner, R. Keeping Cool: Enhanced Optical Reflection and Radiative Heat Dissipation in Saharan Silver Ants. *Science* **2015**, *349* (6245), 298–301.
- (13) Smith, G. B.; Gentle, A. R.; Arnold, M. D.; Gali, M. A.; Cortie, M. B. The Importance of Surface Finish to Energy Performance. *Renew. Energy Environ. Sustain.* **2017**, *2*, 13.
- (14) Wang, T.; Wu, Y.; Shi, L.; Hu, X.; Chen, M.; Wu, L. A Structural Polymer for Highly Efficient All-Day Passive Radiative Cooling. *Nat. Commun.* **2021**, *12* (1), 365.
- (15) Song, J.; Seo, J.; Han, J.; Lee, J.; Lee, B. J. Ultrahigh Emissivity of Grating-Patterned PDMS Film from 8 to 13 μ m Wavelength Regime. *Appl. Phys. Lett.* **2020**, *117* (9), 94101.
- (16) Zhou, L.; Song, H.; Liang, J.; Singer, M.; Zhou, M.; Stegenburgs, E.; Zhang, N.; Xu, C.; Ng, T.; Yu, Z.; Ooi, B.; Gan, Q. A Polydimethylsiloxane-Coated Metal Structure for All-Day Radiative Cooling. *Nat. Sustain.* **2019**, *2* (8), 718–724.
- (17) Castillo, M. E. G.; Patera, A. T. Three-Dimensional Ribbing Instability in Symmetric Forward-Roll Film-Coating Processes. *J. Fluid Mech.* **1997**, *335*, 323–359.
- (18) Chong, Y. H.; Gaskell, P. H.; Kapur, N. Coating with Deformable Rolls: An Experimental Investigation of the Ribbing Instability. *Chem. Eng. Sci.* **2007**, *62* (15), 4138–4145.

- (19) Bauman, T.; Sullivan, T.; Middleman, S. Ribbing Instability in Coating Flows: Effect of Polymer Additives. *Chem. Eng. Commun.* **1982**, *14* (1–2), 35–46.
- (20) Greener, J.; Sullivan, T.; Turner, B.; Middleman, S. Ribbing Instability of a Two-Roll Coater: Newtonian Fluids. *Chem. Eng. Commun.* **1980**, *5* (1–4), 73–83.
- (21) Abbasi, S.; Zebarjad, S. M.; Baghban, S. H. N.; Youssefi, A.; Ekrami-Kakhki, M.-S. Experimental Investigation of the Rheological Behavior and Viscosity of Decorated Multi-Walled Carbon Nanotubes with TiO₂ Nanoparticles/Water Nanofluids. *J. Therm. Anal. Calorim.* **2016**, *123* (1), 81–89.
- (22) Jo, B.; Banerjee, D. Viscosity Measurements of Multi-Walled Carbon Nanotubes-Based High Temperature Nanofluids. *Mater. Lett.* **2014**, *122*, 212–215.
- (23) Islam, M. D.; Perera, H.; Black, B.; Phillips, M.; Chen, M.; Hodges, G.; Jackman, A.; Liu, Y.; Kim, C.; Zikry, M.; et al. Template-Free Scalable Fabrication of Linearly Periodic Microstructures by Controlling Ribbing Defects Phenomenon in Forward Roll Coating for Multifunctional Applications. *Adv. Mater. Interfaces* **2022**, *9*, No. 2201237.
- (24) Fields, R. J.; Ashby, M. F. Finger-like Crack Growth in Solids and Liquids. *Philos. Mag.* **1976**, *33* (1), 33–48.
- (25) Lee, J. H.; Han, S. K.; Lee, J. S.; Jung, H. W.; Hyun, J. C. Ribbing Instability in Rigid and Deformable Forward Roll Coating Flows. *Korea-Australia Rheol. J.* **2010**, *22* (1), 75–80.
- (26) Grillet, A. M.; Lee, A. G.; Shaqfeh, E. S. G. Observations of Ribbing Instabilities in Elastic Fluid Flows with Gravity Stabilization. *J. Fluid Mech.* **1999**, *399*, 49–83.
- (27) Bohren, C. F.; Huffman, D. R. *Absorption and Scattering of Light by Small Particles*; John Wiley & Sons: 2008.
- (28) Li, D.; Liu, X.; Li, W.; Lin, Z.; Zhu, B.; Li, Z.; Li, J.; Li, B.; Fan, S.; Xie, J.; Zhu, J. Scalable and Hierarchically Designed Polymer Film as a Selective Thermal Emitter for High-Performance All-Day Radiative Cooling. *Nat. Nanotechnol.* **2021**, *16* (2), 153–158.
- (29) Mandal, J.; Fu, Y.; Overvig, A. C.; Jia, M.; Sun, K.; Shi, N. N.; Zhou, H.; Xiao, X.; Yu, N.; Yang, Y. Hierarchically Porous Polymer Coatings for Highly Efficient Passive Daytime Radiative Cooling. *Science* **2018**, *362* (6412), 315–319.
- (30) Mandal, J.; Yang, Y.; Yu, N.; Raman, A. P. Paints as a Scalable and Effective Radiative Cooling Technology for Buildings. *Joule* **2020**, *4* (7), 1350–1356.
- (31) Li, X.; Peoples, J.; Yao, P.; Ruan, X. Ultrawhite BaSO₄ Paints and Films for Remarkable Daytime Subambient Radiative Cooling. *ACS Appl. Mater. Interfaces* **2021**, *13* (18), 21733–21739.
- (32) Yu, X.; Chan, J.; Chen, C. Review of Radiative Cooling Materials: Performance Evaluation and Design Approaches. *Nano Energy* **2021**, *88*, No. 106259.
- (33) Li, X.; Sun, B.; Sui, C.; Nandi, A.; Fang, H.; Peng, Y.; Tan, G.; Hsu, P. C. Integration of Daytime Radiative Cooling and Solar Heating for Year-Round Energy Saving in Buildings. *Nat. Commun.* **2020**, *11* (1), 1–9.
- (34) Aili, A.; Yin, X.; Yang, R. Global Radiative Sky Cooling Potential Adjusted for Population Density and Cooling Demand. *Atmosphere (Basel)* **2021**, *12* (11), 1379.
- (35) National Weather Service. <https://www.weather.gov/wrh/Climate?wfo=lot> (accessed on May 4, 2023), Chicago O'Hare international airport weather record.
- (36) Baechler, M. C.; Williamson, J. L.; Gilbride, T. L.; Cole, P. C.; Hefty, M. G.; Love, P. M. *Building America Best Practices Series: Vol. 7.1: Guide to Determining Climate Regions by County*; Pacific Northwest National Lab. (PNNL): Richland, WA, 2010.